



This is a repository copy of *Late Pleistocene acceleration of deformation across the northern Tianshan piedmont (China) evidenced from the morpho-tectonic evolution of the Dushanzi anticline.*

White Rose Research Online URL for this paper:  
<http://eprints.whiterose.ac.uk/131078/>

Version: Supplemental Material

---

**Article:**

Charreau, J., Saint-Carlier, D., Lavé, J. et al. (7 more authors) (2018) Late Pleistocene acceleration of deformation across the northern Tianshan piedmont (China) evidenced from the morpho-tectonic evolution of the Dushanzi anticline. *Tectonophysics*, 730. pp. 132-140. ISSN 0040-1951

<https://doi.org/10.1016/j.tecto.2018.02.016>

---

© 2018 Elsevier B.V. This is an author produced version of a paper subsequently published in *Tectonophysics*. Uploaded in accordance with the publisher's self-archiving policy. Article available under the terms of the CC-BY-NC-ND licence (<https://creativecommons.org/licenses/by-nc-nd/4.0/>)

**Reuse**

This article is distributed under the terms of the Creative Commons Attribution-NonCommercial-NoDerivs (CC BY-NC-ND) licence. This licence only allows you to download this work and share it with others as long as you credit the authors, but you can't change the article in any way or use it commercially. More information and the full terms of the licence here: <https://creativecommons.org/licenses/>

**Takedown**

If you consider content in White Rose Research Online to be in breach of UK law, please notify us by emailing [eprints@whiterose.ac.uk](mailto:eprints@whiterose.ac.uk) including the URL of the record and the reason for the withdrawal request.



[eprints@whiterose.ac.uk](mailto:eprints@whiterose.ac.uk)  
<https://eprints.whiterose.ac.uk/>

Online repository data of "Late Pleistocene acceleration of deformation across the northern Tianshan piedmont (China) evidenced from the morpho-tectonic evolution of the Dushanzi anticline" by Charreau et al.

### Terraces profile evolution including sediment aggradation

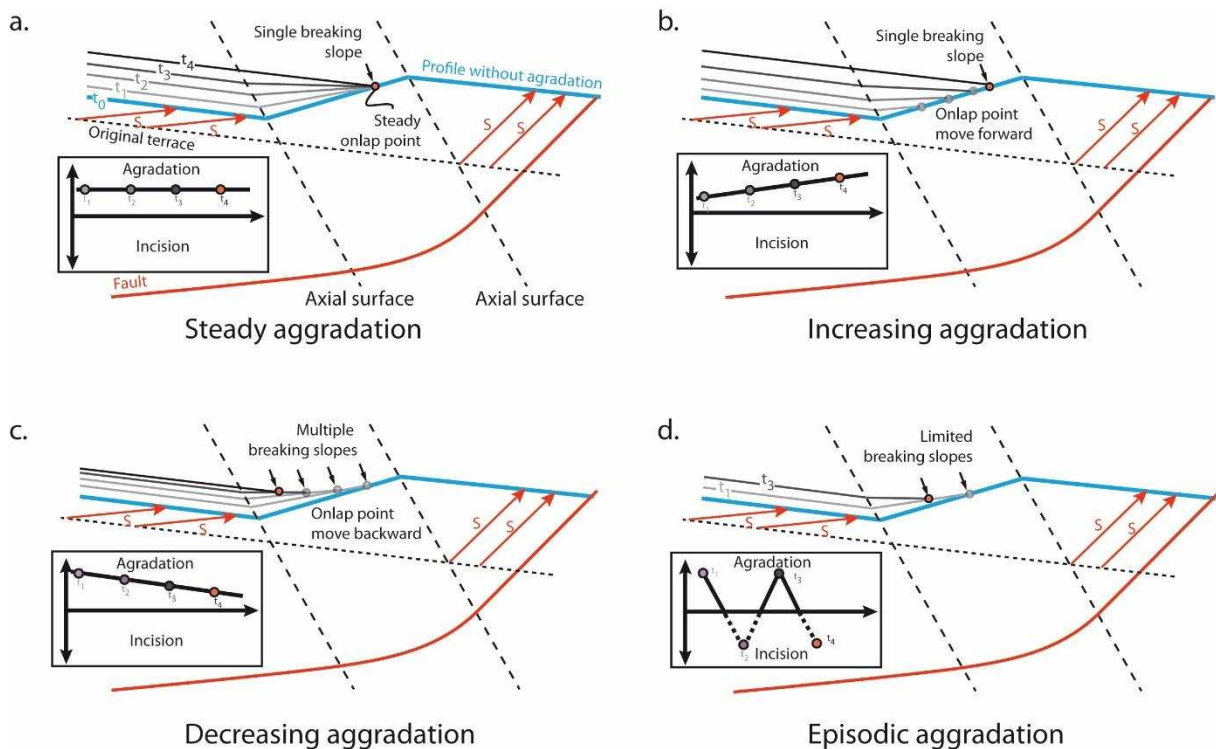


**Fig. A:** Terrace profile evolution during folding when sediment aggradation occurs in the back limb of a fault-bend fold. a. constant aggradation rate; b. increasing aggradation rates; c. decreasing aggradation rate; d. episodic aggradation

### Single grain P-IRSL analyses: sample treatment and measurements

The sample was prepared for extraction of K-feldspar grains of size 175-200  $\mu\text{m}$ . After wet-sieving, the sample was treated with low-concentration HCl to dissolve any carbonates. To isolate the potassic feldspars, the sediment fraction of density  $< 2.565 \text{ g/cm}^3$  was separated with lithium polytungstate (Rhodes, 2014). Lastly, the sample was washed in dilute HF to etch away the outer surface of the grains, thereby increasing their brightness (HCl is also incorporated into this final treatment to suppress the formation of calcium fluoride).

All luminescence measurements were performed at the UCLA luminescence laboratory on a Risø TL-DA-20 automated reader equipped with a single-grain IR laser (Bøtter-Jensen et al., 2003) and a  $^{90}\text{Sr}/^{90}\text{Y}$  beta source. Emissions were detected through a Schott BG3-BG39 filter combination.

Equivalent dose values were obtained following the post-IR IRSL protocol of Buylaert et al. (2009) modified for single-grain stimulation (e.g. Brown et al., 2015). We use a second stimulation temperature of 225  $^{\circ}\text{C}$  to minimize thermal fading while still monitoring a signal that depletes with moderate sunlight exposure (Smedley et al., 2015). The U and Th concentrations were measured with inductively-coupled plasma mass spectrometry (ICP-MS), and the K concentration was measured using inductively-coupled plasma optical emission spectrometry (ICP-OES). The radionuclide concentrations are given in the online depository and were converted to total beta dose-rate using the factors of Adamiec and Aiken (1998).

To correct for the effects of athermal fading (Huntley and Lamothe, 2001), single aliquot measurements of p-IR IRSL signal intensity were made using a beta dose of 55 Gy, a preheat of 250 °C for 60 s (the same preheat used in determining burial dose), and storage at room temperature for up to 13 days. The measured signal loss for the sample studied corresponds to a  $g$ -value of  $2.13 \pm 0.76$  % loss per decade. The final age estimate reported in Table A has been fading-corrected with this  $g$ -value using a/the function supplied in the ‘Luminescence’ package within the **R** programming environment (Kreutzer et al., 2012).

**Table A:** Dosimetry data for individual samples and single-grain post-IR IRSL depositional ages.

Lab code	% K	Th (ppm)	U (ppm)	Depth (m)	Total dose rate (Gy/ka)	Equivalent dose (Gy)	Faded age (ka)	Unfaded age (ka)*
J0467	$2.1 \pm 0.1$	$10.1 \pm 3.2$	$3.17 \pm 0.16$	5.0	$4.169 \pm 0.195$	$395.1 \pm 32.6$	$94.8 \pm 9.2$	$116.1 \pm 14.8$

\*Fading correction performed using measured  $g$ -value of  $2.13 \pm 0.76$  % loss per decade ( $t_c = 3,230$  s).

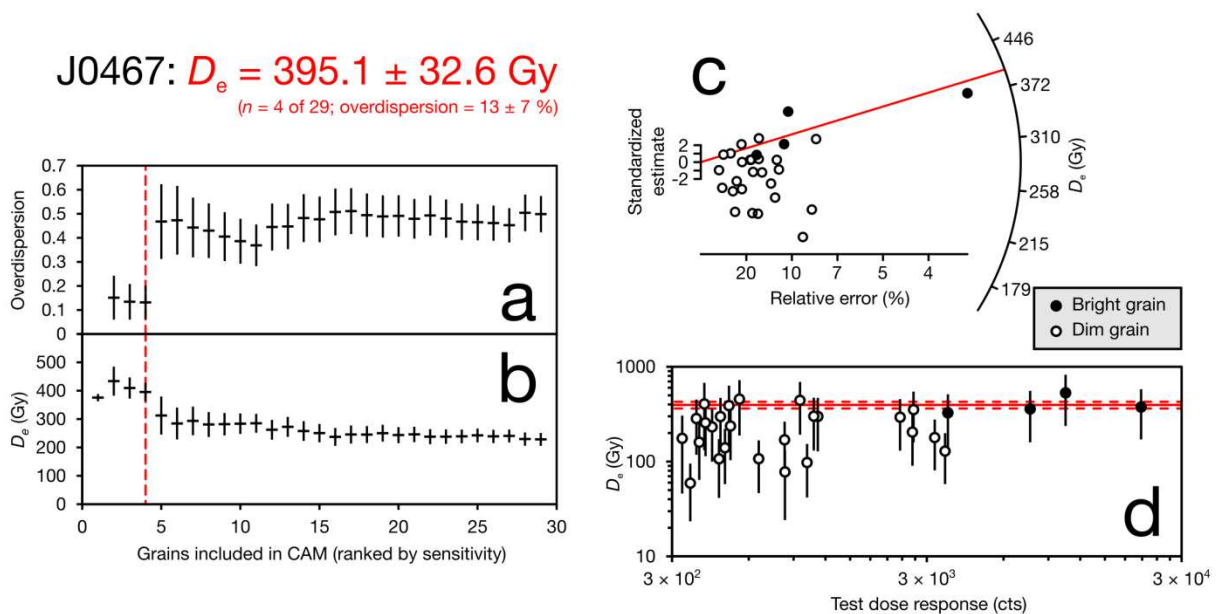


**Fig. B:** Overdispersion (a) and equivalent dose (b) values calculated using the Central Age Model (CAM) plotted as a function of the number of grains included for sample J0465. Grains are ordered by brightness, so that initially only the brightest grain is included, and then the two brightest, and so on. For this sample, we include the 15 brightest grains to calculate an equivalent dose of  $127.2 \pm 9.5$  Gy (this population exhibits an overdispersion characteristic of a well-bleached population and exhibits the lowest relative error); (c) A radial plot showing the bright (i.e. the chosen) grains as filled circles and the dim grains as empty circles. The equivalent dose of the bright population is shown as a red line; (d) A log-log plot of single-grain equivalent dose plotted as a function of grain brightness (test dose response). The sample mean and standard deviation are shown as solid and dashed lines, respectively.

### Cosmogenic $^{10}\text{Be}$ dating of T10

In situ cosmogenic  $^{10}\text{Be}$  is essentially produced by spallation reactions in surface rocks that are impacted by secondary cosmic rays generated in the atmosphere (Dunai, 2010; Gosse and Phillips, 2001). According to Lal (1991), the  $^{10}\text{Be}$  concentration at a single location and a depth ( $z$  in cm) is function of the surface cosmogenic production rate ( $P$  in  $\text{atom g}^{-1} \text{a}^{-1}$ ), the different particle attenuation lengths ( $\Lambda$  in  $\text{g.cm}^{-2}$ ), the radioactive decay of the nuclide considered ( $\lambda$  in  $\text{a}^{-1}$ ), the

erosion rate at the sample location ( $\varepsilon$  in  $\text{cm}\cdot\text{yr}^{-1}$ ), the density of the rocks  $\rho$  ( $\text{g}\cdot\text{cm}^{-3}$ ), the inherited cosmogenic isotope concentration ( $\overline{C}_0$  in atoms), and the exposure time (t in yr):

$$C(z, \varepsilon, t) = \overline{C}_0 \cdot e^{-\lambda t} + \sum_{i=n, m_1, m_2} \frac{P_i}{\frac{\rho \cdot \varepsilon}{\Delta_i} + \lambda} \cdot e^{-\frac{\rho \cdot z}{\Delta_i}} \cdot \left(1 - e^{-\left(\lambda + \frac{\rho \cdot \varepsilon}{\Delta_i}\right) t}\right) \quad (1)$$

where  $n$ ,  $m_1$ , and  $m_2$  refer to the neutrons, slow muons and fast muons, respectively;  $\Delta_n = 160 \text{ g}\cdot\text{cm}^{-2}$ ;  $\Delta_{m1} = 1500 \text{ g}\cdot\text{cm}^{-2}$ ;  $\Delta_{m2} = 4320 \text{ g}\cdot\text{cm}^{-2}$  (Braucher et al., 2011);  $T_{1/2} = 1.387 \text{ Ma}$  (Chmeleff et al., 2010; Korschinek et al., 2010) and  $\lambda = \ln(2)/T_{1/2}$ ;  $\rho = 2.0 \pm 0.2 \text{ g}\cdot\text{cm}^{-3}$ . The local  $^{10}\text{Be}$  production rates were scaled for local latitude and altitude according to Stone (2000). In this study we used the SLHL (see level high latitude) production rate (P) of  $3.9 \pm 0.1 \text{ at}\cdot\text{g}^{-1}\cdot\text{yr}^{-1}$  (Balco et al., 2008; e.g. Kaplan et al., 2011) and the slow ( $0.01 \text{ at}\cdot\text{g}^{-1}\cdot\text{yr}^{-1}$ ) and fast ( $0.034 \text{ at}\cdot\text{g}^{-1}\cdot\text{yr}^{-1}$ ) muonic production rates derived from Braucher *et al.*, (2011). The production rate was scaled to the site location with the scaling of Stone (2000). Based on this formulation and a depth profile of concentration, the age can be inverted using a modeling approach that relies on a least square adjustment, which enables several variables to be tested together (Braucher et al., 2000; Dunai, 2010; Gosse and Phillips, 2001; Hidy et al., 2010; Siame et al., 2004). We used a similar inversion procedure that explores the combination of several unknown variables, including the exposure age (t), the average erosion ( $\varepsilon$ ) and the average inherited concentration ( $C_0$ ). Our technique also accounts for possible depth variability in the inherited concentration (see appendix in Saint-Carlier et al. (2016). The Chi square minimal value ( $\chi_{min}^2$ ) is considered to be the best solution and the uncertainties are defined by the range of values included in  $\chi^2 < \chi_{min}^2 + 1$  (e.g. Siame et al., 2004).

In the case of surface samples only, the general equation can be simplified as:

$$C = C_0 \cdot e^{-\lambda t} + \frac{P_0}{\lambda} \cdot (1 - e^{-\lambda t}) \quad (2)$$

The apparent exposure ages calculated from the surface samples can be then estimated following two extreme hypotheses regarding the inherited component. The inheritance is bracketed between 0  $\text{at}\cdot\text{g}^{-1}$  and the concentration is obtained from the depth profile:

$$-\frac{1}{\lambda} \cdot \ln\left(\frac{\overline{C}_c - \frac{P_0}{\lambda}}{\overline{C}_{0c} - \frac{P_0}{\lambda}}\right) \leq t_{exp} \leq -\frac{1}{\lambda} \cdot \ln\left(1 - \frac{\overline{C}_c \cdot \lambda}{P_0}\right), \text{ with } P_0 = \sum_{i=n, m_1, m_2} P_i \quad (3)$$

This prudent hypothesis is justified since several studies have found evidence for a grain-size dependency in cosmogenic nuclide concentrations in stream sediments in active mountains:  $C_0$  decreases as particle size increases (Brown et al., 1995; Puchol et al., 2014).

Thus, in order to date the abandonment of terrace T3, we combined both approaches and collected 11 samples (Fig. C) for cosmogenic  $^{10}\text{Be}$  analysis: 5 samples were collected along a 5-m-deep vertical profile in the alluvial terrace deposits and the 6 others correspond to cobbles collected at the surface, close to the profile (see table 1 for details). Samples were processed at CRPG in Nancy. Samples were sieved to obtain the 200-800  $\mu\text{m}$  fraction, and quartz was then extracted by magnetic sorting and acid leaching. The quartz separates were then purified in three HF baths to remove atmospheric  $^{10}\text{Be}$  from the grain surfaces and defaults (Brown *et al.*, 1991; Kohl and Nishiizumi, 1992). The purified quartz samples were then completely dissolved in HF after addition of 200  $\mu\text{l}$  of an in-house 2020 ppm  $^9\text{Be}$  carrier solution, with a  $^{10}\text{Be}/^9\text{Be}$  ratio of  $\sim 5 \times 10^{-16}$ . The purified BeO was then obtained following subsequent purification by anion exchange, cation exchange and alkaline precipitations. The  $^{10}\text{Be}/^9\text{Be}$  ratios of these BeO samples were then measured at the French national AMS (Accelerator Mass Spectrometer) facility ASTER (Accelerator for Earth Sciences, Environment and Risks) located at CEREGE (Aix en Provence, France). Ratios were normalized to the  $^{10}\text{Be}/^9\text{Be}$  SRM 4325 NIST reference material using an assigned value of  $(2.79 \pm 0.03) \times 10^{-11}$  (Nishiizumi et al., 2007). This standardization is equivalent to 07KNSTD within rounding error. All results are given in

Table B. The mean  $^{10}\text{Be}/^9\text{Be}$  ratio of 22 chemical blank samples was  $1.7 \pm 0.7 \times 10^{-15}$ . Blank corrections represent between  $\sim 4\%$  and  $31\%$  of the samples (average =  $16\%$ ).

The cosmogenic  $^{10}\text{Be}$  depth profile does not display a clear exponential decrease. This probably results from a variable and high inherited  $^{10}\text{Be}$  component compared to the amount of  $^{10}\text{Be}$  produced since the deposition of the terrace material. Excluding the 40-cm-deep sample that is a  $2\sigma$  outlier, the concentrations in  $^{10}\text{Be}$  (Table 1) provide a poorly defined exponential best-fit, indicating that the terrace was abandoned  $6_{-6}^{+11}$  kyr ago (Fig. C).

The probability density function (PDF) of each of the surface cobbles are plotted in figure C along with the samples of (Molnar et al., 1994), which were updated with the revised production rate and the most recent AMS standardization (Nishiizumi et al., 2007). The data are quite scattered, reflecting the variable inheritance of the cobbles (due to distinct initial exposure times or their elevation on the hillslope of the contributing watershed). We averaged the concentrations in order to smooth out these variable inheritances and produce a virtual amalgamated sample. The first solution, which assumes no inheritance, yields a maximum age estimate of  $14.5 \pm 2.7$ . The second solution, which is based on the average inheritance of the sandy material calculated from the depth profile ( $64 \pm 13 \times 10^3 \text{at.g}^{-1}$ ), constrains the terrace abandonment to a minimum age of  $6.9 \pm 3.3$  ka. As the inheritance seems to decrease as the sediment grain size increases (e.g. Brown et al., 1995; Puchol et al., 2014), the inheritance of the cobbles might be smaller than the value extracted from the depth profile (where samples are essentially sand). The abandonment age of the terrace is therefore most likely older than this minimum value. In any case, the estimated 'surface cobble age' (between 6 and 15 ka) is in agreement with the age derived from the depth profile. It is also in agreement with the previous CRN and luminescence ages carried out on T3 (Malatesta et al., 2017; Poisson and Avouac, 2004).

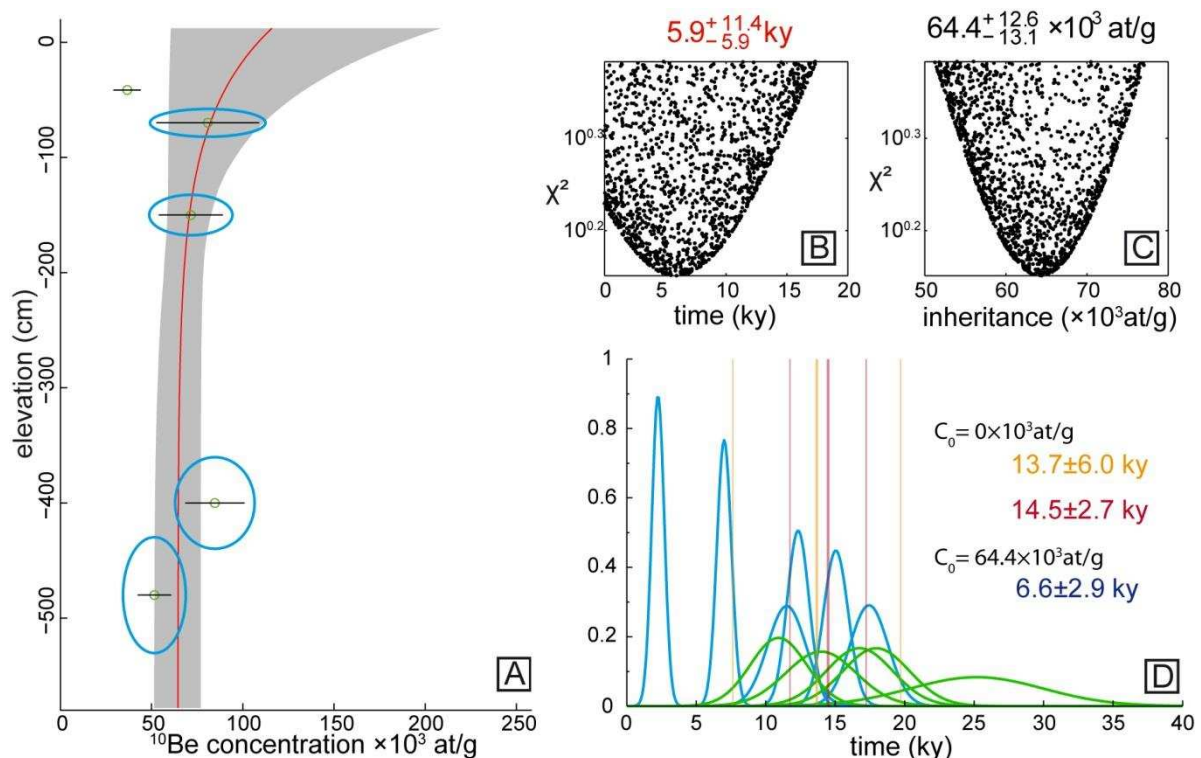


**Fig. C:** A: Cosmogenic depth profile on T10 with  $^{10}\text{Be}$  concentration plotted against the depth. The red line represents the best modeled profile assuming null erosion and the gray envelope is the  $1\sigma$  uncertainty. B and C: Chi square values as a function of time and inheritance, respectively. D: Probability distribution of surface cobble ages assuming null inheritance. The green and blue curves

represent the recalculated data from Molnar et al., (1994) and our own data, respectively. The orange lines refer to the mean and the standard deviation of all the data. The red lines show the same information when the outliers at  $2\sigma$  are excluded from the calculation. The blue value corresponds to the mean and standard deviation (without outliers) when we take into account the inheritance of the depth profile and apply it to the surface samples.

**Table B:** Cosmogenic results.

sample name	depth (cm)	thickness depth (cm)	sample type	pure Qz weight (g)	$^{10}\text{Be}/^9\text{Be}$ $10^{-14}$	$^{10}\text{Be}$ counts	$^{10}\text{Be}$ concentration $10^3(\text{at/g})$	error $10^3(\text{at/g})$
Kuitun (44.3005°N, 84.7763°E, Z = 828 m)								
TS10_KTN_T10_P0a	0	5	granite cobble	12.32	8.88	286	96.2	6.2
TS10_KTN_T10_P0b	0	5	granite cobble	22.59	6.21	201	54.7	4.1
TS10_KTN_T10_P0c	0	5	Qz cobble	4.06	2.98	101	89.9	10.8
TS10_KTN_T10_P0e1	0	5	granite cobble	17.66	1.69	33	17.6	3.5
TS10_KTN_T10_P0e2	0	5	granite cobble	6.20	6.42	221	135.9	10.7
TS10_KTN_T10_P0e3	0	5	granite cobble	9.87	8.62	488	117.3	6.9
TS10_KTN_T10_P1	40	10	sand and fine pebbles	4.24	1.44	60	36.5	7.3
TS10_KTN_T10_P2a	70	10	sand and fine pebbles	1.69	0.84	15	80.8	28.1
TS10_KTN_T10_P3	150	10	sand and fine pebbles	1.82	0.81	38	71.5	17.6
TS10_KTN_T10_P4	400	10	sand and fine pebbles	1.83	1.45	63	84.7	16.3
TS12_KTN_T10_P5	480	20	sand and fine pebbles	2.17	1.01	69	51.6	9.3

## Fold modeling

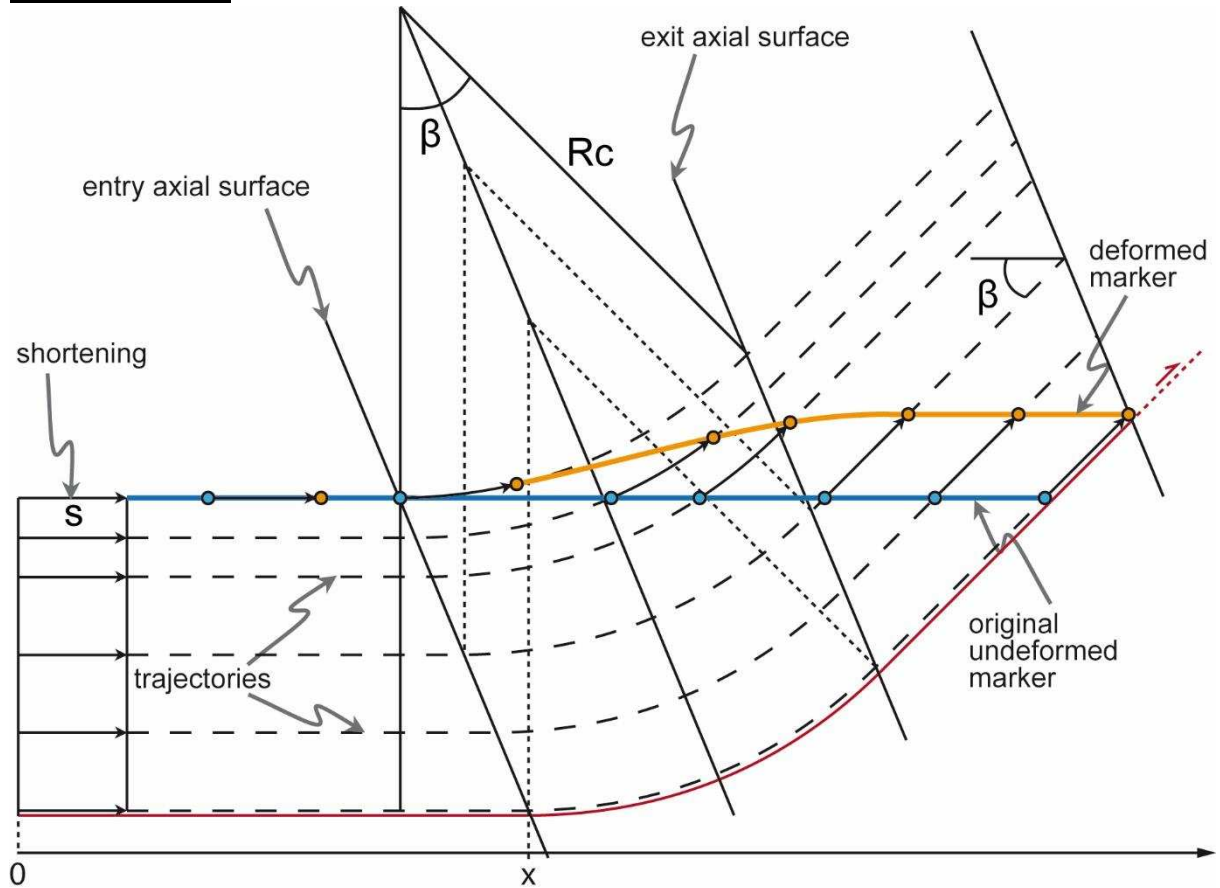


**Fig. D:** Model geometry based on the curved-hinge kinkband migration principle in which folding takes place progressively as particles move through the active hinge zone. According to this model and the curved fold geometry with  $R_c$  the radius of curvature and  $\beta$  the opening angle, the new coordinates  $X, Z$  can be calculated after an increment of slip  $S$  on the horizontal décollement.

## Seismic data and treatment

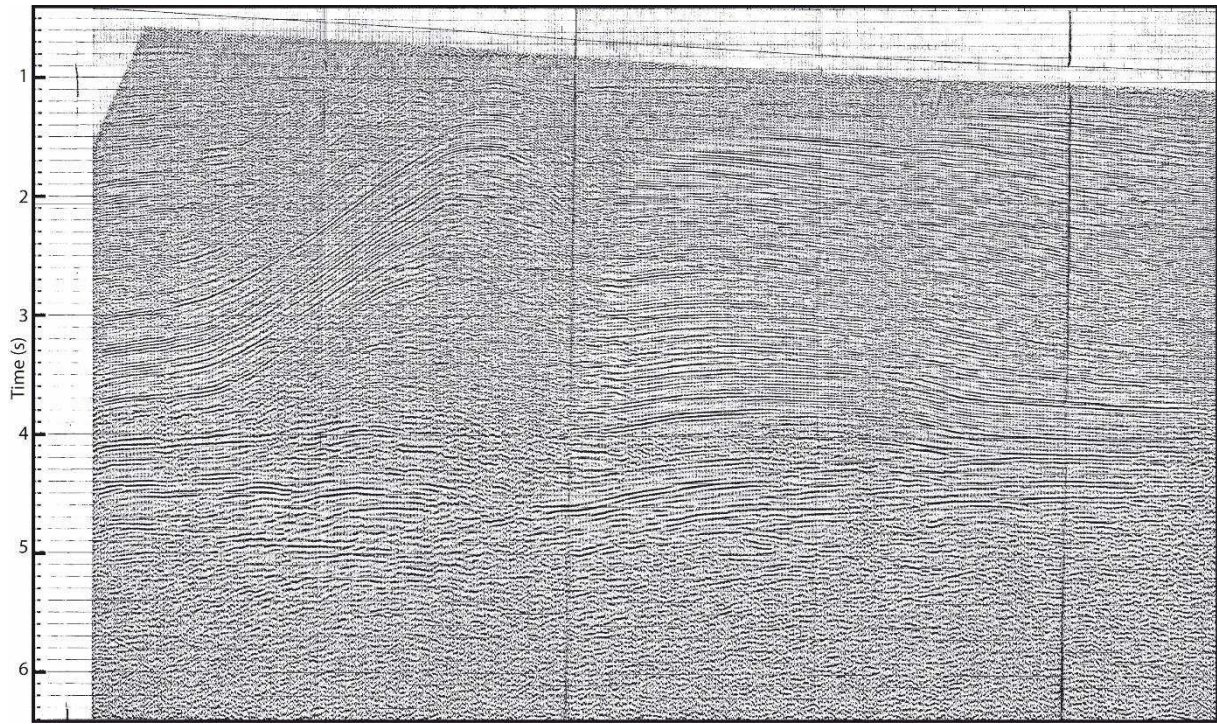


**Fig. E:** Seismic line provided by the Chinese oil field company and used to constrain the depth geometry of the fold model.

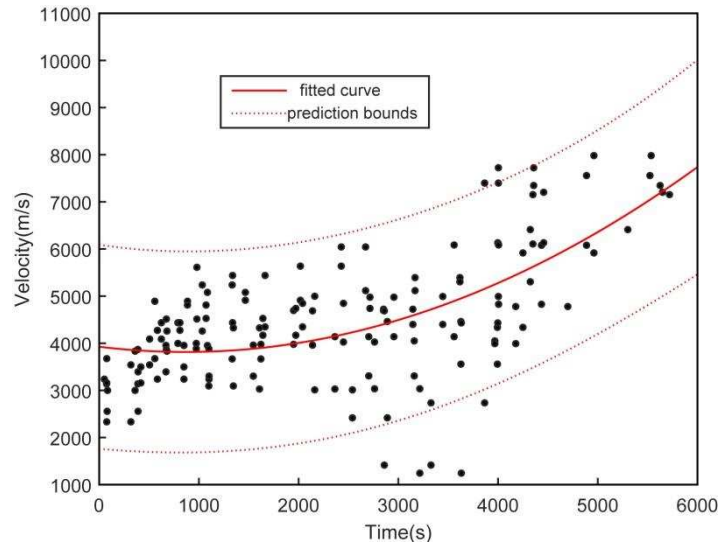


**Fig. F:** Velocity-time data and fitted law used to migrate the seismic line to depth.

## Bibliography

- Adamiec, G., Aitken, M.J., 1998. Dose-rate conversion factors: update. *Anc. TL* 37–50.
- Balco, G., Stone, J.O., Lifton, N.A., Dunai, T.J., 2008. A complete and easily accessible means of calculating surface exposure ages or erosion rates from  $^{10}\text{Be}$  and  $^{26}\text{Al}$  measurements. *Quat. Geochronol.* 3, 174–195. doi:10.1016/j.quageo.2007.12.001
- Bøtter-Jensen, L., Andersen, C.E., Duller, G.A.T., Murray, A.S., 2003. Developments in radiation,

- stimulation and observation facilities in luminescence measurements. *Radiat. Meas.* 37, 535–541. doi:10.1016/S1350-4487(03)00020-9
- Braucher, R., Bourlès, D.L., Brown, E.T., Colin, F., Muller, J.-P., Braun, J.-J., Delaune, M., Minko, A.E., Lescouet, C., Raisbeck, G.M., Yiou, F., 2000. Application of in situ-produced cosmogenic  $^{10}\text{Be}$  and  $^{26}\text{Al}$  to the study of lateritic soil development in tropical forest: theory and examples from Cameroon and Gabon. *Chem. Geol.* 170, 95–111.
- Braucher, R., Merchel, S., Borgomano, J., Bourlès, D.L., 2011. Production of cosmogenic radionuclides at great depth : A multi element approach. *Earth Planet. Sci. Lett.* 309, 1–9. doi:10.1016/j.epsl.2011.06.036
- Brown, E.T., Stallard, R.F., Larsen, M.C., Raisbeck, G.M., Yiou, F., 1995. Denudation rates determined from the accumulation of in situ produced  $^{10}\text{Be}$  in the Luquillo experimental forest, Puerto-Rico. *Earth Planet. Sci. Lett.* 129, 193–202.
- Brown, N.D., Rhodes, E.J., Antinao, J.L., McDonald, E. V., 2015. Single-grain post-IR IRSL signals of K-feldspars from alluvial fan deposits in Baja California Sur , Mexico. *Quat. Int.* 362, 132–138. doi:10.1016/j.quaint.2014.10.024
- Chmeleff, J., von Blanckenburg, F., Kossert, K., Jakob, D., 2010. Determination of the  $^{10}\text{Be}$  half-life by multicollector ICP-MS and liquid scintillation counting. *Nucl. Instruments Methods Phys. Res. Sect. B Beam Interact. with Mater. Atoms* 268, 192–199.
- Dunai, T.J., 2010. *Cosmogenic Nuclides*. Cambridge University Press, Cambridge.
- Gosse, J.C., Phillips, F.M., 2001. Terrestrial in situ cosmogenic nuclides : theory and application. *Quat. Sci. Rev.* 20, 1475–1560.
- Hidy, A.J., Gosse, J.C., Pederson, J.L., Mattern, J.P., Finkel, R.C., 2010. A geologically constrained Monte Carlo approach to modeling exposure ages from profiles of cosmogenic nuclides: An example from Lees Ferry, Arizona 11. doi:10.1029/2010GC003084
- Huntley, D.J., Lamothe, M., 2001. Ubiquity of anomalous fading in K-feldspars and the measurement and correction for it in optical dating 1106, 1093–1106. doi:10.1139/cjes-38-7-1093
- Kaplan, M.R., Strelin, J.A., Schaefer, J.M., Denton, G.H., Finkel, R.C., Schwartz, R., Putnam, A.E., Vandergoes, M.J., Goehring, B.M., Travis, S.G., 2011. In-situ cosmogenic  $^{10}\text{Be}$  production rate at Lago Argentino , Patagonia : Implications for late-glacial climate chronology. *Earth Planet. Sci. Lett.* doi:10.1016/j.epsl.2011.06.018
- Korschinek, G., Bergmaier, A., Faestermann, T., Gerstmann, U.C., Knie Rugel, G., K., Wallner, A., Dillmann, I., Dollinger, G., Lierse von Gosstowski, C., Kossert, K., Maiti, M., Poutivtsev, M., Remmert, A., 2010. A new value for the  $^{10}\text{Be}$  half-life by Heavy-Ion Elastic Recoil detection and liquid scintillation counting. . *Nucl. Inst. Meth. B* 268, 187–191.
- Kreutzer, S., Schmidt, C., Fuchs, M.C., Dietze, M., Fischer, M., Fuchs, M., 2012. Introducing an R package for luminescence data analysis. *Anc. TL* 30, 1–8.
- Lal, D., 1991. Cosmic ray labeling of erosion surfaces: in situ nuclide production rates and erosion models. *Earth Planet. Sci. Lett.* 104, 424–439.
- Malatesta, L.C., Avouac, Jean-Philippe Brown, N.D., Breitenbach, S.F.M., Pan, J., Chevalier, M.-L., Rhodes, E., Saint-Carlier, Dimitri Zhang, W., Charreau, J., Lavé, J., Blard, P.-H., 2017. Lag and mixing during sediment transfer across the Tian Shan piedmont caused by climate-driven aggradation-incision cycles. *Bull. Geol. Soc. Am.* In press.
- Molnar, P., Brown, E.T., Burchfiel, B.C., Deng, Q., Feng, X., Li, J., Raisbeck, G.M., Shi, J., Wu, Z., Yiou, F., You, H., 1994. Quaternary Climate Change and the Formation of River Terraces across Growing Anticlines on the North Flank of the Tien Shan, China. *J. Geol.* 102, 583–602.
- Nishiizumi, K., Imamura, M., Caffee, M.W., Southon, J.R., Finkel, R.C., McAninch, J., 2007. Absolute calibration of  $^{10}\text{Be}$  AMS standards. *Nucl. Instruments Methods Phys. Res. Sect. B-Beam Interact. with Mater. Atoms* 258, 403–413.
- Poisson, B., Avouac, J.P., 2004. Holocene hydrological changes inferred from alluvial stream entrenchment in North Tian Shan (Northwestern China). *J. Geol.* 112, 231–249.
- Puchol, N., Lavé, J., Lupker, M., Blard, P.-H., Gallo, F., France-Lanord, C., 2014. Grain-size dependent concentration of cosmogenic  $^{10}\text{Be}$  and erosion dynamics in a landslide-dominated Himalayan

- watershed. *Geomorphology* 224, 55–68. doi:10.1016/j.geomorph.2014.06.019
- Rhodes, E.J., 2014. Dating sediments using potassium feldspar single-grain IRSL : Initial methodological considerations. *Quat. Int.* 1–9. doi:10.1016/j.quaint.2014.12.012
- Saint-Carlier, D., Charreau, J., Lavé, J., Blard, P.H., Dominguez, S., Avouac, J.-P., Wang, S., Arnold, M., Aumaître, G., Keddadouche, K., Léanni, L., Chauvet, F., Bourlés, D.L., 2016. Major temporal variations in shortening rate absorbed along a large active fold of the southeastern Tianshan piedmont (China). *Earth Planet. Sci. Lett.* 434, 333–348. doi:10.1016/j.epsl.2015.11.041
- Siame, L., Bellier, O., Braucher, R., Sébrier, M., Cushing, M., Bourlès, D., Hamelin, B., Baroux, E., Voogd, B. De, Raisbeck, G., Yiou, F., 2004. Local erosion rates versus active tectonics : cosmic ray exposure modelling in Provence ( south-east France ) 220, 345–364. doi:10.1016/S0012-821X(04)00061-5
- Smedley, R.K., Duller, G.A.T., Roberts, H.M., 2015. Bleaching of the post-IR IRSL signal from individual grains of K-feldspar: implications for single-grain dating. *Radiat. Meas.* 79, 33–42. doi:10.1016/j.radmeas.2015.06.003
- Stone, J.O., 2000. Air pressure and cosmogenic isotope production. *J. Geophys. Res. - Solid Earth* 105, 23753–23759.